Journal of Energy Storage 61 (2023) 106791

Contents lists available at ScienceDirect

Journal of Energy Storage

journal homepage: www.elsevier.com/locate/est

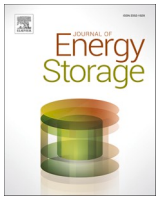

Research papers

Comparative investigation of the thermal runaway and gas venting behaviors of large-format $LiFePO_4$ batteries caused by overcharging and overheating

Zhuangzhuang Jia [a], Shuping Wang [b], Peng Qin [a,*], Changhao Li [b], Laifeng Song [a], Zhixiang Cheng [a], Kaiqiang Jin [a], Jinhua Sun [a], Qingsong Wang [a,*]

[a] State Key Laboratory of Fire Science, University of Science and Technology of China, Hefei 230026, PR China
[b] State Grid Anhui Electric Power Research Institute, State Grid Laboratory of Fire Protection for Transmission and Distribution Facilities, Anhui Province Key Laboratory of Electric Fire and Safety Protection, Hefei 230601, PR China

ARTICLE INFO

Keywords:
$LiFePO_4$ battery
Lithium-ion battery safety
Thermal runaway
Gas venting
Overcharging
Overheating

ABSTRACT

With the large-scale application of $LiFePO_4$ (LFP) batteries in the field of electrochemical energy storage (EES), more attention is being paid to the problem of thermal runaway (TR). This paper investigates the TR and gas venting behaviors of 86 Ah LFP batteries caused by overcharging and overheating. Compared with previous studies, the main contributions lie in the gas venting behavior analysis of the LFP batteries during the whole TR process and the causes of the safety venting under overcharging and overheating. Two significant results are obtained from the experiments: (I) the overcharging of the LFP battery promotes gas release inside the battery, resulting in advance of safety venting, but the safety venting under overheating is caused by electrolyte volatilization; (II) the total gas volume (including H_2, CH_4, C_2H_4, CO and CO_2) during TR under overcharging and overheating is 62.1 and 101.3 L. Moreover, the results calculated by the fractional compelling dose model show that there is no toxicity before TR under overheating. However, the duration of toxicity under the overcharge is 1211 s before TR. This work provides a meaningful theoretical guide for EES systems' safety warning and fire protection.

Nomenclature

Symbols

LIB	lithium-ion battery
EES	electrochemical energy storage
TR	thermal runaway
SOC	state of charge
LFP	$LiFePO_4$
NCM	$LiNi_{1/3}Co_{1/3}Mn_{1/3}O_2$
FTIR	Fourier transform infrared
P	pressure (Pa)
P_{in}	total pressure inside the battery (Pa)
P_{gas}	the partial pressure of gas release (Pa)
c	specific heat capacity (J/mol/K)
T	temperature (°C)
T_{avg}	average temperature (°C)
T_{up}	temperature of the upper surface (°C)
T_{mid}	temperature of the middle surface (°C)
T_{down}	temperature of lower surface (°C)
T_{onset}	onset temperature of TR (°C)
T_{max}	maximum temperature of TR (°C)
$(dT/dt)_{max}$	maximum self-heat rate (°C/s)
ISC	internal short circuit
X_{FED}	the critical concentration of irritant gas
P_{ele}	the partial pressure of electrolyte volatilization (Pa)
Δt	the time interval between the safety venting and the end of TR (s)
OCV	open circuit voltage
C	current rates
SEI	solid electrolyte interphase
EC	ethylene carbonate
DMC	dimethyl carbonate
EMC	ethyl methyl carbonate

* Corresponding authors.
E-mail addresses: pengqin@ustc.edu.cn (P. Qin), pinew@ustc.edu.cn (Q. Wang).

https://doi.org/10.1016/j.est.2023.106791
Received 13 October 2022; Received in revised form 5 January 2023; Accepted 27 January 2023
Available online 11 February 2023

CMC	carboxy methylcellulose
PVDF	polyvinylidene fluoride
V_{total}	total gas volume (L)
U	voltage (V)
$\overline{\dot{m}}$	the average mass loss rate (g/s)
m	mass (g)
m_{loss}	the mass loss during TR (g)
t	time (s)
t_{SV}	time of the safety venting (s)
t_{ISC}	time of internal short circuit (s)
t_{onset}	onset time of the TR (min)
t_d	thermal runaway duration (s)
$t_{d@jet}$	duration of jet behavior (s)
FED	fractional effective dose

Greeks

ϕ	the concentration of gas (ppm)

1. Introduction

With the energy crisis and environmental pollution problems becoming increasingly severe, developing and utilizing clean and renewable energy are imperative [1–3]. The lithium-ion battery (LIB) is considered an advanced energy storage medium for renewable energy [4]. Owing to the perfect combination of its high energy density, low self-discharge rate, and excellent cycle performance, LIBs have been widely used in electrochemical energy storage (EES) systems [2,5]. According to incomplete statistics, as of 2021, China's EES scale of operation had reached 1.87 GW, and the cumulative installed capacity reached 5.51 GW, with an increase of 68.5 % year on year. Among them, LIBs have occupied the largest incremental installation scale [6]. However, in the past 10 years, there have been 32 major fire and explosion accidents in EES systems around the world, including three fire accidents in EES systems in China [7], such as the Beijing energy storage station fire accident in April 2021. LIB is one of the core components of EES systems, whose safety issues are becoming technical hindrances for the development of the EES industry.

Thermal runaway (TR) is the primary safety issue of LIBs [8]. It is a chemical reaction accompanied by heat generation and gas release [9]. Fig. 1 shows a diagram of the potential causes of LIB accidents. TR can be induced by mechanical, electrical, or thermal abuse [10]. A series of battery safety tests with TR have been extensively studied. These tests include mechanical [11,12], electrical [13], and thermal tests [14]. Huang et al. [15] experimentally investigated the characteristics and mechanisms of TR in $LiNi_{1/3}Co_{1/3}Mn_{1/3}O_2$ (NCM) batteries caused by overcharging and overheating. They found that compared with TR under overheating, TR induced by overcharging exhibited a more severe result because of its higher heat generation. Lai et al. [10] compared the TR propagation behaviors of LIB modules under overheating, nail penetration, and overcharging. The energy flow distribution shows that more than 60 % of TR energy is used for battery self-heating.

Furthermore, several researchers have studied the TR behaviors of $LiFePO_4$ (LFP) batteries caused by overcharging or overheating. Wang et al. [16] studied the effects of the current rate and health state on TR characteristics under overcharging and analyzed the TR behavior and the overcharge voltage curve variation. A realistic energy storage pack TR experiment was established by Sun et al. [17]. The TR process of the LFP module was tested and explored under two overcharging conditions. Liu et al. [18] studied the TR and fire behaviors of batteries under overheating. They analyzed the composition and type of gas production and fire behavior of the different state of charge (SOC) batteries. Bugryniec et al. [19] investigated the TR mechanism of LFP batteries with different SOCs and found that at SOC of 100 % and 110 %, the anode and cathode reactions are the main contributors to TR; while at lower SOC, anode reaction dominates.

In previous studies [20,21], researchers have conducted many TR experiments on LIBs under overcharging and overheating, but most studies have focused on battery fire behavior. Due to the cathode material properties of NCM batteries, the NCM battery causes fire behavior during TR. The fire behavior of NCM batteries is exceptionally well studied. However, LFP batteries are dominant in energy storage plants in China because the LFP battery cannot ignite in the open space during TR. Therefore, the previous work did not guide battery accidents in EES stations.

LFP batteries release large amounts of fumes during TR. So, it is necessary to study the gas venting behavior of LFP batteries. Previous studies on gas generation have focused on placing the test sample into a closed canister and then measuring the internal pressure during TR [22,23]. The gas generation rate was calculated from the gas state

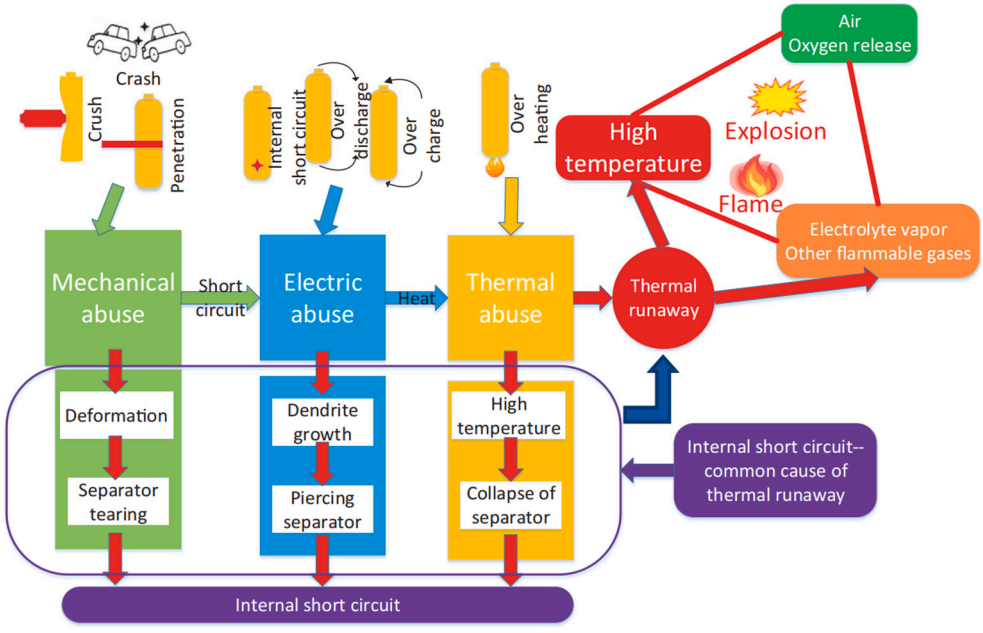

Fig. 1. Diagram of the causes of LIB accidents [4].

equation based on the changes in pressure. Yih-Shing Duh et al. [24] compared the TR behavior of commercial 14,500, 18,650 and 26,650 $LiFePO_4$ batteries in an accelerating rate calorimeter through a closed canister and found that the maximum pressure of 26,650 was about 4.5 bar. Golubkov et al. [25] demonstrated the TR characteristics of three types of commercial 18,650 LIBs and found the types of gas generation were CO_2, CO, H_2, CH_4, C_2H_4 and C_2H_6 during TR. Recent research is only for a single trigger method for overheating or overcharging. The overheating and overcharging triggers of LIBs have an enormous impact on the TR behavior, especially for the more severe effect on the gas venting behavior of the LFP battery. However, there is a gap in the gas venting behavior under overcharging and overheating. Comparative studies of the TR characteristics and mechanisms of LFP batteries under overcharging and overheating are still lacking. Therefore, it is necessary to investigate the TR and gas venting behaviors of LFP batteries under overcharging and overheating.

This work investigates the TR and gas venting behaviors of 86 Ah commercial prismatic LIBs under overcharging and overheating. The present work and previous research are partially summarized in Table 1. Some critical parameters of TR are revealed in detail. The causes for the safety venting of the LFP batteries and the impact of the safety venting are analyzed under overcharging and overheating. This work reveals the TR behavior and mechanism of LFP batteries in EES under overcharging and overheating, which provides reference data for the design of fire prevention and emergency disposal of EES accidents.

2. Experimental

2.1. The $LiFePO_4$ battery sample

The sample is a commercial large-scale commercial LFP battery used in the EES station. The physical dimensions of the LFP battery are shown in Table 2. The cathode active material is $LiFePO_4$, while the anode is graphite. The nominal capacity and voltage are 86 Ah and 3.2 V. Before the experiment, all batteries were fully charged by using a battery cycler (NEWARE CT-4004-30V50A-NFA). Each tested LIB is charged at a rate of 20 A (0.23C) to 3.65 V using a constant current and voltage (CC-CV). After charging is completed, the battery is maintained for 24 h to ensure stability.

2.2. Experimental apparatus

This experiment was conducted in the combustion chamber, which was fabricated following ISO 9705 and ISO 5660 [27,28]. The combustion chamber size is 1.8 m × 1.8 m × 2 m. The diagram of the combustion chamber is shown in Fig. 2(a). A smoke exhaust duct on the upper side of the combustion chamber and an airflow of 279 L/s are maintained to remove gas from the combustion chamber during the test.

Table 2
The physical parameters of the LFP battery.

Name	Unit	Value
Cathode	–	Lithium phosphate ($LiFePO_4$)
Anode	–	Graphite
Dimension(length × width × height)	mm^3	205 × 175 × 30
Safety vent size (length × width)	mm^2	10 × 20
Nominal capacity	Ah	86
Maximum cut-off voltage	V	3.65
Minimum cut-off voltage	V	2.5
Nominal voltage	V	3.2
maximum charge/discharge current	A	86
Operating temperature range	°C	−20–55
Mass	g	1979.8
State of charge	%	100
Specific heat capacity	J/kg/K	1029

Fourier transform infrared (FTIR) spectroscopy and an independent hydrogen probe were arranged in the exhaust duct to monitor the composition and content of the gases. The gas concentration and content were obtained by a Thermo Scientific™ Antaris™ IGS Gas Analyser and an independent hydrogen analysis instrument.

The tested battery was placed on a Mettler balance in the combustion chamber. The balance data were used to record the mass loss of the LFP battery during TR. K-type thermocouples were attached to the surface of the battery to measure its surface temperature. High-temperature tapes ensure good contact between the thermocouple and the battery surface in the experiment. In addition, a thermocouple was placed 4 mm above the safety vent to monitor the temperature of the ejected gas. The locations of the thermocouples are shown in Fig. 2. Temperature data were recorded by the data acquisition equipment (ICPCON I-7018). During the test, a video camera (SONY XPS160) was used to monitor TR behavior and the gas injection phenomenon.

2.3. TR tests under overheating and overcharging conditions

(I) Overcharging condition

In the experiment, a 0.5C (43 A) constant current charging method was used to trigger the TR of the LFP battery. The upper and lower voltage limits were not set during overcharging to ensure that the battery could fail. With the excessive energy input from the battery cycler, the voltage kept changing until the battery ultimately failed. The voltage dropped to near 0 V. The experiment was finished.

(II) Overheating condition

A heating plate with a constant power of 500 W was used to trigger the TR of the tested battery. The size of the heating plate (205 × 175 ×

Table 1
A summary of the research on the TR of LFP batteries and this work.

No.	Ref.	length × width × height (mm)	Capacity (Ah)	Trigger method	Charging rate/ heating power	Results
1	[16]	173 × 19 × 140	25	Overcharging	1C	The voltage curve has five obvious inflection points during the overcharge process.
2	[17]	LIB module	344	Overcharging	0.5C	As the battery module fails, it generates an intense flame and a large amount of high-temperature smoke, which contains H_2, CO, CO_2, HCl, HF, SO_2, and other components.
3	[18]	100 × 20 × 140	22	Overheating	500 W	This paper stated the SOC has a more significant effect on TR behavior, and the jet fire is blown out for a fully charged battery. The production of CO and HF increases with the increase of SOC.
4	[26]	148 × 27 × 90	27	Overheating	400 W	The maximum injection velocity occurs at the moment of the safety venting with a value of 42.05 m/s.
5	[27]	180 × 70 × 205	300	Overheating	500 W	This paper evaluated the TR and fire hazard of large LFP batteries and compared battery fires to pool and gas fires with standard fuels.
6	This work	205 × 175 × 30	86	Overcharging/ overheating	0.5C/500 W	The TR and gas venting behaviors of large LFP batteries were studied and evaluated under overcharging and overheating, and the gas venting and heat generation of the batteries were analyzed.

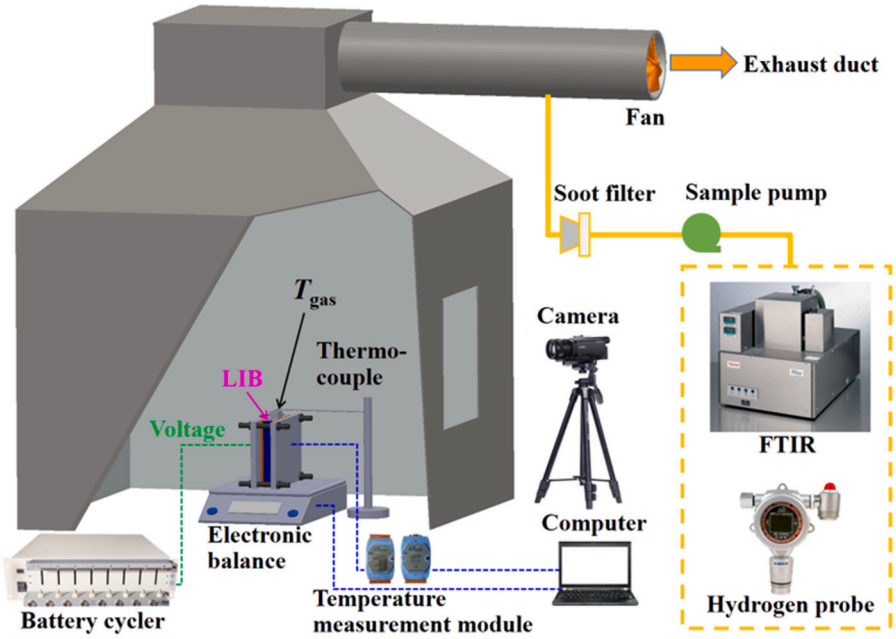

(a) Experimental equipment

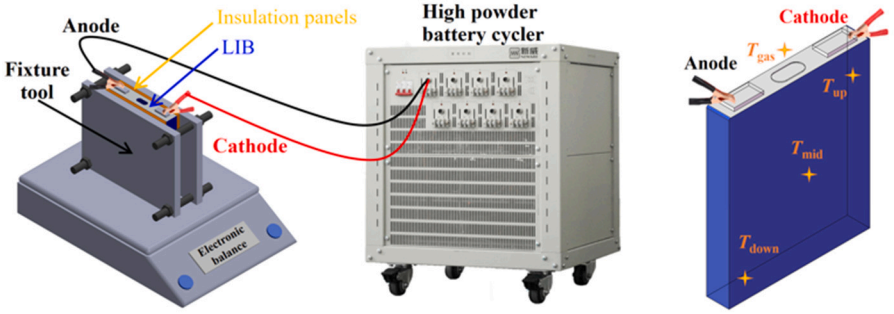

(b) Experimental arrangement of overcharging and thermocouple layout diagram

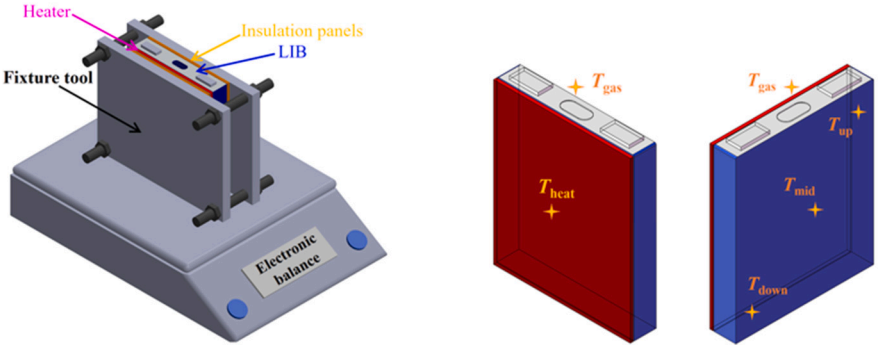

(c) Experimental arrangement of overheating and thermocouple layout diagram

Fig. 2. Overview of the experiment: (a) experimental equipment; (b) experimental arrangement of overcharging and thermocouple layout diagram; (c) experimental arrangement of overheating and thermocouple layout diagram.

3.5 mm) was the same as the contact surface of the battery. The battery and the heating plate were wrapped in thermal insulation cotton with low thermal conductivity. Then, the wrapped battery and the heating plate are clamped with an iron fixture, which can maintain full contact and reduce battery expansion during TR.

3. Results and discussion

3.1. TR behaviors under overcharging and overheating

Fig. 3 shows the typical jet behaviors of the LFP battery under overcharging and overheating. According to the TR behavior, the TR

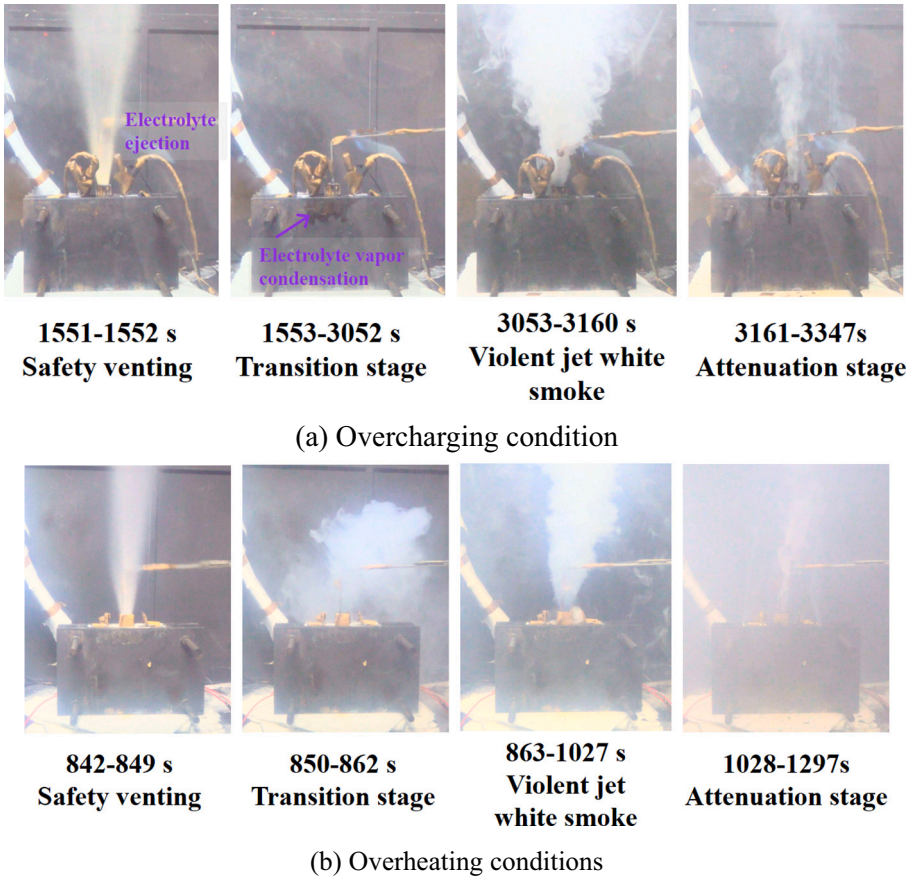

Fig. 3. TR behavior of the $LiFePO_4$ batteries under overcharging and overheating.

process of the two triggering methods can be divided into four stages: safety venting, transition stage, violent jet, and attenuation stage. In the first stage, for the overcharging condition, the safety vent opens at 1551 s, when the surface temperature of the battery is 48.5 °C. The safety vent opens for only 1 s, and a large amount of liquid is emitted. For the overheating condition, the safety vent opens at 842 s when the battery surface temperature is 94 °C. The safety vent opens, releasing a large amount of white smoke over some time. Through previous studies [22,29], the reason for safety venting is the pressure increase inside the LFP battery, which is caused by electrolyte volatilization and gas release inside the battery, as shown in Eq. (1).

$$P_{in} = P_{ele} + P_{gas} \tag{1}$$

where P_{in} represents the total pressure inside the LFP battery, P_{ele} represents the partial pressure generated by electrolyte volatilization, and P_{gas} refers to the partial pressure of gas released inside the battery. The predominant reason for the safety venting of the LFP battery is the electrolyte volatilization under overheating, according to Ref. [30]. It can also be seen from the experiment that the temperature of the safety venting is much higher than the boiling point of the electrolyte when the safety vent opens. However, for the overcharging condition, when the safety vent opens, the surface temperature is 48.5 °C, and the electrolyte ejects as a liquid. Overcharging promotes gas production inside the battery, which also shows that the main reason for the safety venting is caused by the gas release of the LFP battery.

In the second stage, the battery does not show gas jet behavior. After the safety venting, the battery ejects some substances, and the temperature of the battery is significantly reduced. This stage lasts for 999 s under overcharging. There are two main reasons: one is that the safety vent opens to eject a large amount of electrolyte, which removes part of the heat; the other is that the internal temperature of the battery is lower when the safety venting occurs, and it does not reach the temperature of the TR. However, for the overheating condition, this stage lasts only 10 s before the battery undergoes gas injection.

In the third stage, the injection becomes more intense as the chemical reactions intensify inside the battery. Gas ejection is the primary source of the amount of gas released. The durations of jet behavior for the overcharging and overheating conditions are 107 and 164 s, respectively. The critical time points and TR duration under overcharging and overheating are shown in Table 3. The peak temperature of the released gas under overcharging and overheating is almost equal. However, the duration of the gas jet under overheating is longer, and the volume of gas release is larger. In the fourth stage, the TR behavior gradually declines, and the experiment is over.

3.2. Voltage and temperature variation

As shown in Fig. 4, the TR process under overcharging can be divided into four stages, depending on the voltage change [16]. The changes in surface temperature and voltage of the battery are described below in detail. The surface temperature of the battery is considered to be the average of three thermocouple measurements located diagonally across the cell at different heights.

Table 3
Critical time point of TR stages and TR duration under overcharging and overheating.

Time	t_{SV}	t_{ISC}	t_{onset}	t_{max}	$t_{d@jet}$	t_d
Overheating	842 s	912 s	916 s	1097 s	164 s	181 s
Overcharging	1551 s	2512 s	3040 s	3226 s	107 s	186 s

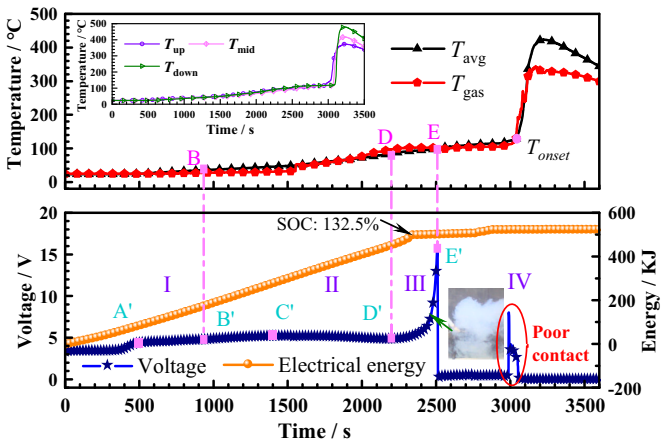

Fig. 4. Variations in temperature, voltage and electrical energy with the time under overcharging.

$$T_{avg} = \frac{T_{up} + T_{mid} + T_{down}}{3} \tag{2}$$

Stage I: at this stage, the voltage rises from 3.36 to 4.53 V (A′) in 0–498 s, and the T_{up} of the battery ranges from 23.5 to 30.8 °C. It can be known that the total resistance ($R_{battery}$) increases greatly after overcharge. The batteries generate much Joule heat ($Q = I^2 R_{battery} t$) during overcharging, where Q represents the heat generated, i is current, $R_{battery}$ is the total battery resistance, and t is time. A great part of electrical energy from the constant current overcharge is converted into Joule heat in the form [31]. Due to the redundant design of the anode, lithium ions are continuously embedded in the anode [32], but the cathode is already in a lithium deficit state, so it is difficult for the anode to obtain lithium ions from the cathode. Therefore, the $R_{battery}$ rises to bring an increase in voltage [16]. The voltage rises from 4.53 (A′) to 4.78 V (B′) in 499–936 s, and the T_{avg} of the cell increases from 24.8 to 35.8 °C. The heat of this process mainly comes from the Joule heat and reaction heat during the overcharge process, where the reaction heat includes the heat generated by lithium-ion deposition in the anode, the reaction heat of lithium precipitation, and the reaction heat of lithium precipitation and electrolyte [33].

Stage II: at this stage, when the voltage rises to 4.78 V, a significant inflection point appears in the voltage curve [34]. Since the cathode is in a lithium-deficient state, the anode can only obtain lithium ions from the electrolyte. While the anode is saturated with lithium ions and cannot accommodate more lithium ions, excess lithium ions can only produce precipitation on the anode, producing lithium metal [35,36]. Lithium metal can be consumed in reaction with the solid electrolyte interphase (SEI) film, resulting in a voltage drop [37]. The voltage at this time reflects the dynamic balance between the anode's precipitation and consumption of lithium ions. The voltage rises from 4.78 (B′) to 5.24 V (C′) in 937–1392 s, and the precipitation of lithium ions dominates. However, the voltage in this stage drops from 5.24 (C′) to 4.88 V (D′), which is caused by the dominance of the reaction between the precipitated lithium and the active material inside the battery at this time [37]. It is worth noting that when $T_{avg} = 49.2$ °C and $U = 5.18$ V, the temperature increase causes the chemical reaction inside the battery to release gas, which also causes the pressure to rise. After the safety venting, the battery's internal temperature is higher than the fixture temperature, and the generated electrolyte vapor condenses on the fixture surface, as shown in Fig. 3(a).

Stage III: the voltage rises from 4.88 V (D′) to 16.50 V (E'), and T_{avg} increases from 87.5 (D) to 99.6 °C (E). The most significant feature of this stage is the rapid increase in voltage due to the partial shrinkage and collapse of the separator. Due to the rapid rise in voltage, more Joule heat is generated, causing an increase in temperature and accelerating the TR side reaction [31,38]. In this stage, T_{gas} is significantly greater than T_{avg}. The gas release process is also more pronounced.

Stage IV: the voltage drops from 16.50 (E') to 0.31 V, and the voltage fluctuates violently between 0 V and 8 V. The voltage drop indicates that partial melting of the separator leads to the occurrence of the internal short circuit (ISC) [39,40]. However, TR does not occur at a voltage drop of 0.31 V, so voltage monitoring of the battery is just perfect for early warning. The source of heat in this stage is mainly due to the side reactions of the battery, which include reactions of cathode and electrolyte, anode and electrolyte, electrolyte decomposition, and internal short circuit exotherm. With the accumulation of heat inside the battery, the battery gradually reaches the TR temperature (T_{onset}) value, and the battery starts to undergo TR. The separator melts completely, and a massive ISC occurs inside the battery, accompanied by a violent redox reaction. The gas release behavior reaches a climax with the phenomenon of smoke jets, which leads to a gradual reduction in visibility inside the entire experimental platform cavity. The violent gas venting behavior causes poor contact between the cathode and anode, which in turn causes violent fluctuations in the voltage [41].

In the overheating condition, the voltage behavior is relatively simple, as shown in Fig. 5. There is a slight voltage fluctuation at 864–897 s, which is mainly due to the separator of jelly roll 1 collapsing. As shown in Fig. 6, the single LIB has two jelly rolls. The slight voltage drop in Fig. 5 is caused by the collapse of the separator of jelly roll 1 and the induced micro-ISC due to the parallel connection of the two jelly rolls. At 909 s, all the layers and the separator of jelly roll 2 are destroyed, or no electrolyte remains in the battery, eliminating the electrochemical system and the voltage drops to 0 V.

Fig. 7 shows the temperature versus the rate of temperature rise under overcharging and overheating. The temperature rise rate appears to have two peak rates of temperature rise under overcharging and overheating. The peak rate of temperature occurs earlier under overheating because the battery receives more heat by the heat transfer than the Joule heat under overcharging. The separator is easier to melt under overheating, and the internal material of the battery is more active; chemical reactions are more likely to occur. However, the two peak rates of temperature rise are higher under overcharging, and the temperature range of the TR is also more extended because the electrical energy input is 517.4 kJ before TR and the SOC of the battery is 132.5 %. The battery produces more heat energy under overcharging.

The peak surface temperature of the battery during TR under overcharging and overheating is 423 and 372.1 °C, respectively, and the peak temperature of gas release is 342.4 and 343.4 °C, respectively. These measured parameters, such as T_{max} and $(dT/dt)_{max}$, are greatly affected by the experimental conditions, as shown in Table 4. Similar

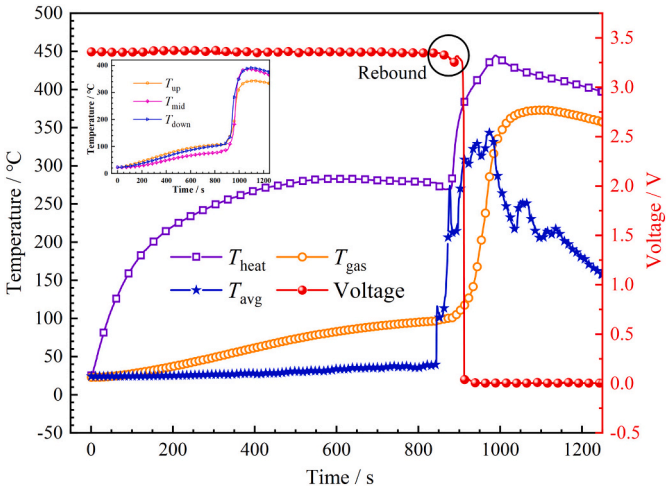

Fig. 5. The variation in temperature and voltage with time under overheating.

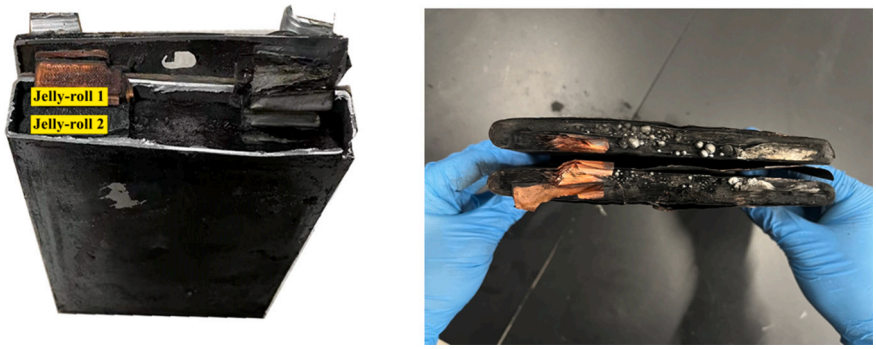

(a) The LFP battery after TR (b) Two jelly rolls from the disassembled LIB.

Fig. 6. Autopsy pictures of failed $LiFePO_4$ battery.

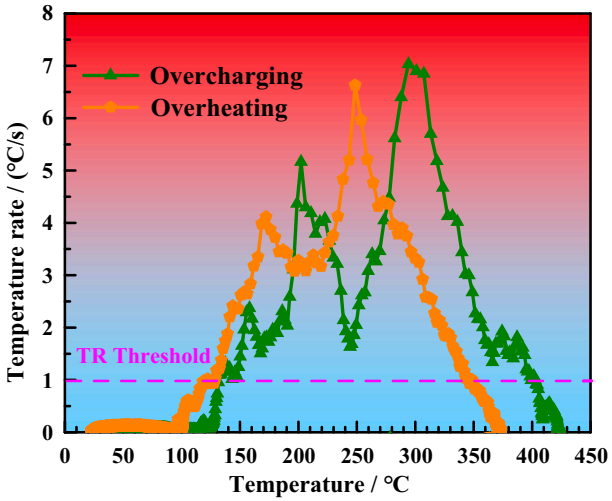

Fig. 7. The variation in the average temperature rate with the average surface temperature under overcharging and overheating.

studies have been performed in some previous articles, and the conclusions are similar to this paper's conclusions. In particular, their $(dT/dt)_{max}$ values are maintained at 4.1–9.1 °C/s, which ensures the accuracy and reliability of the experimental data.

3.3. Gas analysis and toxicity assessment

3.3.1. Gas composition analysis

The LFP battery does not generate flames during TR, so the gas released from the battery is vital for gas composition analysis. The gas composition and gas release volume during TR under overcharging and overheating are analyzed by a hydrogen detector and FTIR spectroscopy. The leading gases released were detected as CO_2, C_2H_4, H_2, CO and CH_4, as shown in Fig. 8. Huang et al. [43] analyzed the gas generation composition of LFP batteries, and the gas composition was highly consistent with this paper. The gas generation is mainly caused by the reactions of the active materials of the cathode, the embedded active lithium ions, the binder, the SEI film, the electrolyte and the separator, and these reactants at high temperatures.

The earliest generated CO_2 is from the thermal decomposition of the substable material of the SEI film [30,44]. The reaction of the SEI film with H_2 and HF also produces CO_2. Furthermore, the reaction between the electrolyte and O_2 releases large amounts of CO_2. Taking ethylene carbonate (EC) as an example [45–47]:

$$(CH_2OCOLi)_2 \rightarrow Li_2CO_3 + C_2H_4 + CO_2 + \frac{1}{2}O_2 \quad (3)$$

$$ROCO_2Li + HF \rightarrow ROH + CO_2 + LiF \quad (4)$$

$$2ROCO_2Li + H_2 \rightarrow 2ROH + Li_2CO_3 + CO_2 \quad (5)$$

$$\frac{5}{2}O_2 + 2C_3H_4O_3(EC) \rightarrow 3CO_2 + 2H_2O \quad (6)$$

The EC is susceptible to reduction reactions on the lithium-rich anode to produce C_2H_4, and the decomposition of the SEI film also produces C_2H_4 [48,49]:

$$2Li + C_3H_4O_3(EC) \rightarrow Li_2CO_3 + C_2H_4 \quad (7)$$

$$2Li + (CH_2OCO_2Li)_2 \rightarrow 2Li_2CO_3 + C_2H_4 \quad (8)$$

The primary source of CO is due to the reduction of CO_2 by active lithium ions from the anode to generate Li_2CO_3 and CO [50,51]. Moreover, the electrolyte is also susceptible to the reduction of active lithium ions under high-temperature conditions to generate CO [52]:

$$2CO_2 + 2Li^+ + 2e^- \rightarrow Li_2CO_3 + CO \quad (9)$$

Table 4
Summary and comparison of the thermal characteristics of the LFP batteries.

No.	Ref.	Capacity	Size	OCV or SOC	Trigger method	T_{onset} (°C)	T_{max} (°C)	$(dT/dt)_{max}$ (°C/s)	With flame or not
1	[23]	0.9 Ah	14,500	3.7 V	Overheating	205.5	253.8	1.2	Without
2	[24]	1.1 Ah	18,650	4.2 V	ARC	207.6	295.7	0.37	Without
3	[24]	2.5 Ah	26,650	4.2 V	ARC	204.8	386	9.7	Without
4	[16]	25 Ah	Prismatic	3.3 V	Overcharging	101.1	335	N/A	Without
5	[26]	27 Ah	Prismatic	100 %	Overheating	149.6	405	5.2	Without
6	[42]	228 Ah	Prismatic	100 %	Overcharging	159.4	649.8	9.1	With
7	[27]	300 Ah	Prismatic	100 %	Overheating	150.2	573.1	4.1	Without
8	This work	86 Ah	Prismatic	3.4 V	Overcharging	138.4	423.6	7.1	Without
9	This work	86 Ah	Prismatic	100 %	Overheating	117.5	373.1	6.6	Without

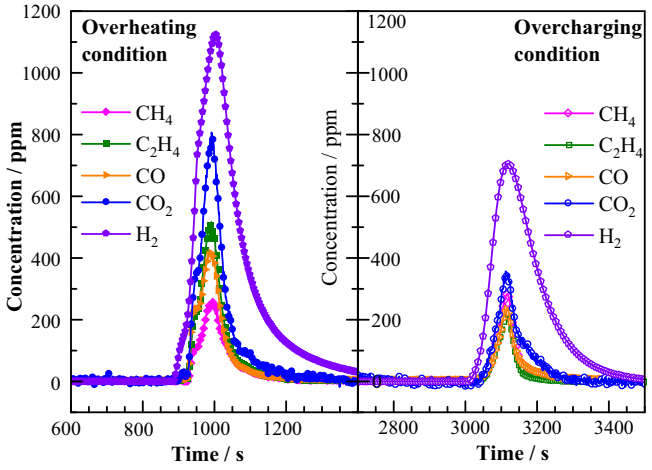

Fig. 8. The variation in the gas concentration of TR under overcharging and overheating.

$$DMC + 2e^- + 2Li^+ \rightarrow 2CH_3OLi + CO \quad (10)$$

$$EC + 2e^- + 2Li^+ \rightarrow (CH_2OLi)_2 + CO \quad (11)$$

The reaction between the binder and the lithium ion is considered an essential source of H_2. When the temperature exceeds 230 °C, the graphite particles on the anode fall off, allowing direct contact between the lithium metal and the binder [53]. While the commonly used materials for the binder are polyvinylidene fluoride (PVDF) and carboxy methyl cellulose (CMC), under high-temperature conditions, PVDF and CMC react with lithium metal in direct contact [30,54]:

$$PVDF + Li \rightarrow LiF + -CH=CF- + \frac{1}{2}H_2 \quad (12)$$

$$CMC + Li \rightarrow CMC\text{-}OLi + \frac{1}{2}H_2 \quad (13)$$

CH_4 is generated due to the reduction of dimethyl carbonate (DMC) by H_2 to produce CH_4 [49,52,55]:

$$DMC + Li^+ + e^- + \frac{1}{2}H_2 \rightarrow CH_3OCO_2Li + 2CH_4 \quad (14)$$

$$DMC + 2Li^+ + 2e^- + H_2 \rightarrow Li_2CO_3 + 2CH_4 \quad (15)$$

The released gases of the whole TR process under overcharging and overheating are summed, as shown in Table 5. CO_2 and H_2 account for the majority of the released gases, which is the same conclusion as in Ref. [25]. The total gas volume under overheating is greater than the amount of each gas under overcharging. The total gas production of the battery is calculated, and the total gas generations are 62.1 and 101.3 L under overcharging and overheating, Yuan et al. [29] carried out the calculation of gas release volume for a 3.8 Ah LFP battery, which yielded 3.79, 8.98, and 11.72 L for 1 battery, 2 batteries, and 3 batteries, respectively. This also indirectly reflects that the amount of gas release in this paper is reasonable. Due to the battery receives more heat transfer from outside under overheating, the internal reaction of the battery is more violent and the time of gas release is longer. The electrolyte volatilization of the battery is larger under overcharging. So, the gas venting volume is more under overheating.

Table 5
The comparison of gas compositions during TR under overcharging and overheating.

Gases compositions (L)	H_2	CO_2	CO	C_2H_4	CH_4	Total
Overcharging condition	30.7	10.3 L	7.9 L	7.0 L	6.2 L	62.1 L
Overheating condition	47.4 L	22.7 L	11.5 L	12.3 L	7.4 L	101.3 L

3.3.2. Toxicity assessment

The toxic-gas model described in an international standard (ISO 13571) is employed to evaluate the toxicity of ejected gases under overcharging and overheating [43]. It is an excellent method for the quantitative assessment of overall toxicity and has been widely used to assess the fire toxicity of building materials, upholstery materials and even vehicles [56]. Asphyxiation is a key parameter in this approach and its effect can be assessed by determining the effective dose (FED), calculated by Eqs. (16)–(17). X_{FED} is the critical concentration of each irritant gas that is expected to seriously impair the viability of the occupants, as provided by the standard ISO 13571.

$$X_{FED} = \sum_{t_1}^{t_2} \frac{v_{co_2}\phi_{co}}{35000}\Delta t + \sum_{t_1}^{t_2} \frac{(v_{co_2}\phi_{HCN})^{2.36}}{1.2\times 10^6}\Delta t \quad (16)$$

$$v_{CO_2} = exp([CO_2]/5) \quad (17)$$

where ϕ is the concentration of each gas (ppm), and $[CO_2]$ is the average volume percent of CO_2. When the X_{FED} reaches 1, it is expected that 50 % of individuals cannot perform cognitive and motor skill functions at an acceptable level.

Fig. 9 shows the calculated X_{FED} variation during TR under overcharging and overheating. The cumulative effect of asphyxiating gases can be seen in Fig. 9, and the rapid increase in the X_{FED} curve corresponds to the TR of the battery under overcharging and overheating. The peak value of X_{FED} for the overheating condition is 11.6, which is much higher than the 7.7 for the overcharging condition. The toxicity under overheating is much greater than that under overcharging. However, interestingly, the X_{FED} under overheating is less than 1 before TR, and the gas asphyxiation in the environment is small, but the X_{FED} of gas release is more than 1 under overcharging when TR occurs before 1211 s. It is vital for the evaluation of gas release. The harmful gas released from the battery remains severe after the safety venting under overcharging, even if the battery does not suffer from TR.

3.4. Mass loss and mass loss rate

The mass loss and mass loss rate of batteries under overcharging and overheating are shown in Fig. 10. Due to the reaction force exerted on the electronic balance by the gas ejected when the safety vent opens, there is a rebound in the mass loss value under overheating.

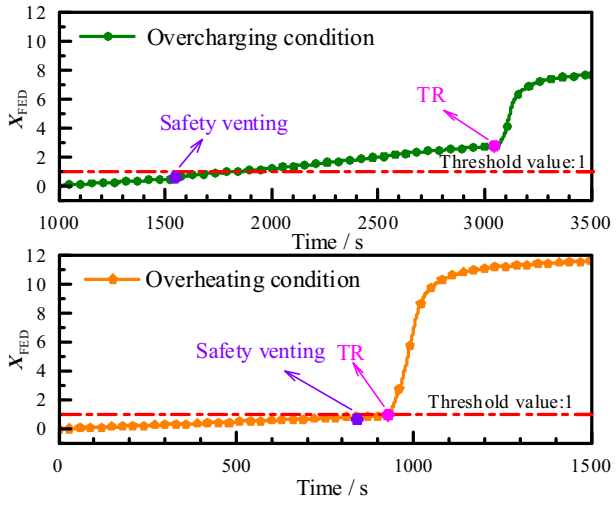

Fig. 9. Assessment of the asphyxiant gases during TR under overcharging and overheating.

Interestingly, when the safety vent opens under overcharging, the battery ejects a large amount of yellow liquid electrolyte, and there is no rebound in the mass loss value. There are two leading causes: (I) the safety vent opens to release more solid and liquid substances under overcharging, and the mass loss is more significant, but the battery mainly releases smoke under overheating, so the mass loss is less. (II) When the safety vent opens under overheating, the temperature of the battery is high, the reaction inside the battery is more intense, and the released gas and electrolyte volatilization cause the internal pressure to rise faster. However, the battery internal pressure increases mainly owing to the reaction of gas release under overcharging, so the pressure rise rate of the battery is lower, so the impact of safety venting is relatively small.

The total mass losses are 419.2 and 403.3 g under overcharging and overheating, respectively, which indicates that the difference in total mass loss is small under overcharging and overheating. Qin et al. [55] evaluated the mass loss of 86 Ah LFP battery and showed the mass loss was 437 ± 45 g under overheating, which is in good agreement with the results of this paper. The mass loss rate is greatly affected by the two triggering methods. In particular, the mass loss rate has two peaks under overcharging and overheating. The two peak mass loss rates are −0.53 and − 1.84 g/s under overcharging, but the peak mass loss rates are −4.3 and − 5.7 g/s under overheating, which is related to the gas release behavior of the batteries. The gas release rate under overheating is much larger than the gas release rate under overcharging. Due to the different times of safety venting under overcharging and overheating, the average rate of mass loss is defined by Eq. (18).

$$\overline{\dot{m}} = \frac{m_{\text{loss}}}{\Delta t} \tag{18}$$

where $\overline{\dot{m}}$ is the average mass loss rate (g/s), m_{loss} is the mass loss during TR (g), and Δt is the time interval between the safety venting and the end of TR (s). The average mass loss rates are 0.24 and 2.25 g/s under overcharging and overheating. This indicates that the two trigger methods significantly affect the mass flow, and the TR of the LFP battery under overheating has a higher average mass loss rate. The TR under overheating is more dangerous.

3.5. Error analysis

Three identical experiments were conducted in two trigger modes to ensure the accuracy and reliability of the experimental data. The average values and the standard deviation of these key parameters are presented in Fig. 11. The standard deviations of these measured parameters, such as $T_{\max}$, T_{onset}, and V_{total}, were less than 10 %. Moreover, the M_{loss} and t_{onset} were repeated well during TR with a standard deviation less than 5 %.

4. Conclusions

This work comparatively investigates the TR and gas venting behaviors of LIBs under overcharging and overheating. Several important parameters, such as temperature, jet behavior and gas composition were obtained and analyzed. The following conclusions can be drawn from this study.

(1) The cause of the safety venting is analyzed under overcharging and overheating. Electrolyte volatilization inside the battery leads to safety venting under overheating, but safety venting is primarily caused by gas release under overcharging. The overcharging of the LFP battery promotes gas release, resulting in the advance of safety venting.

(2) The analysis of gas production is mainly carried out from the internal reaction mechanism of the battery, and the leading gases produced are detected as CO_2, C_2H_4, H_2, CO and CH_4; the total gas volumes are 62.1 and 101.28 L under overcharging and overheating. The peak value of X_{FED} under overheating is 11.6, which is much higher than the 7.7 under overcharging. There is

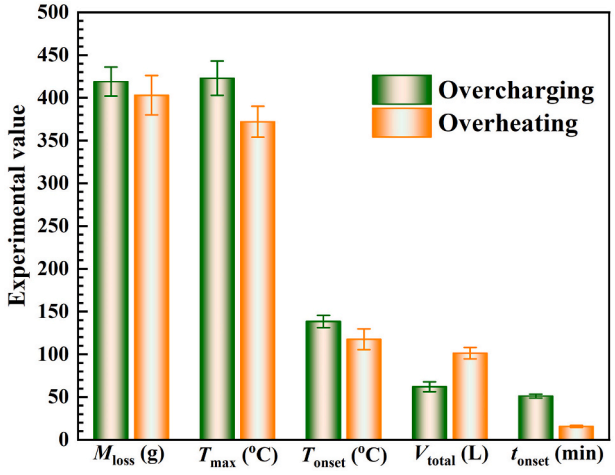

Fig. 11. The error bars of the critical parameters.

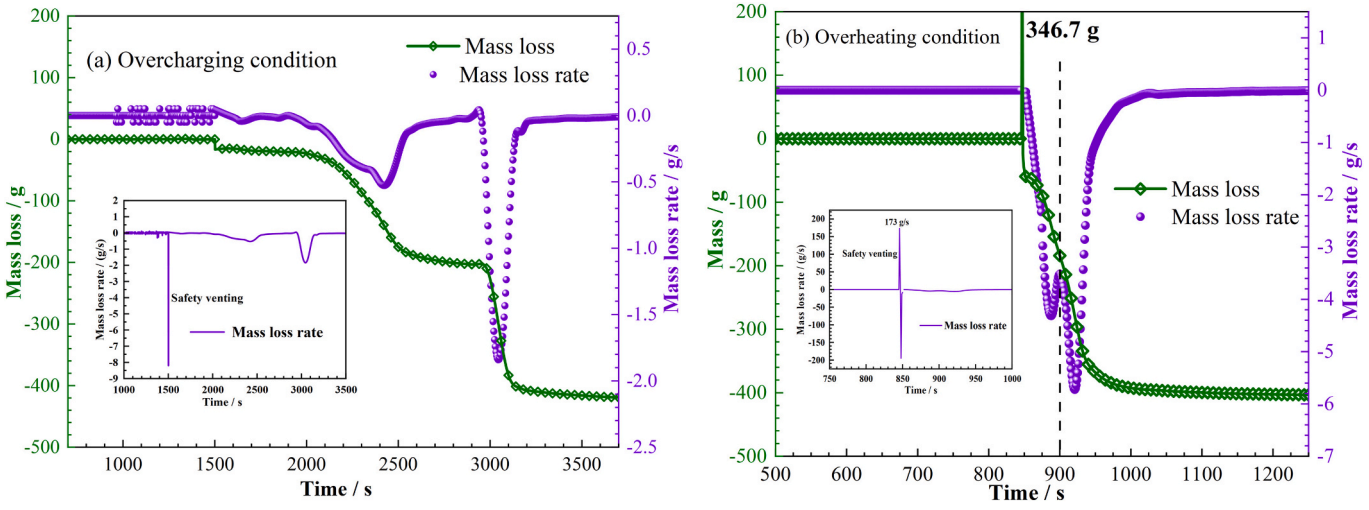

Fig. 10. Mass loss and mass loss rate of batteries under overcharging and overheating.

no toxicity before TR under overheating. However, the duration of toxicity under the overcharge is 1211 s before TR.

(3) The difference in total mass loss is small under overcharging and overheating, but the mass loss rate is greatly affected by the two triggering methods. The two peak mass loss rates are −0.53 and − 1.84 g/s under overcharging, but the peak mass loss rates are −4.3 and − 5.7 g/s under overheating, which reveals that the mass flow and gas release rates are greater under overheating than under overcharging. The TR under overheating is more dangerous.

This work provides essential data and effective theoretical guidance for EES systems' safety warning and fire protection using LFP batteries. Moreover, it can provide guidance for the safe design of large-format LFP energy storage modules.

CRediT authorship contribution statement

Zhuangzhuang Jia: Investigation, Writing - original draft, Data curation, Conceptualization, Writing-review and Editing. **Shuping Wang:** Writing-review and Editing. **Peng Qin**: Visualization, Methodology. **Changhao Li**: Experiments. **Laifeng Song**: Experiments. **Zhixiang Cheng**: Experiments. **Kaiqiang Jin**: Supervision, Writing-review and Editing. **Jinhua Sun**: Supervision, Methodology. **Qingsong Wang**: Writing-Reviewing, Editing, Supervision, Funding acquisition and Project administration.

Declaration of competing interest

The authors declare that they have no known competing financial interests or personal relationships that could have appeared to influence the work reported in this paper.

Data availability

No data was used for the research described in the article.

Acknowledgments

This work is supported by the National Key Research and Development Program of China (No. 2021YFB2402001), Anhui Provincial Natural Science Foundation (No. 2108085UD04), Postgraduate Innovation and Entrepreneurship Practice Project of Anhui Province (No. 2022cxcysj013), the China Postdoctoral Science Foundation (No.2022T150615). Prof. Q.S Wang is supported by Youth Innovation Promotion Association CAS (No. Y201768).

References

[1] X. Zhang, Z. Li, L. Luo, Y. Fan, Z. Du, A review on thermal management of lithium-ion batteries for electric vehicles, Energy 238 (2022), 121652, https://doi.org/10.1016/j.energy.2021.121652.

[2] P. Lyu, X. Liu, J. Qu, J. Zhao, Y. Huo, Z. Qu, et al., Recent advances of thermal safety of lithium ion battery for energy storage, Energy Storage Mater. 31 (2020) 195–220, https://doi.org/10.1016/j.ensm.2020.06.042.

[3] F. Wang, J.D. Harindintwali, Z. Yuan, M. Wang, F. Wang, S. Li, et al., Technologies and perspectives for achieving carbon neutrality, Innovations 2 (4) (2021), 100180, https://doi.org/10.1016/j.xinn.2021.100180.

[4] Q. Wang, B. Mao, S.I. Stoliarov, J. Sun, A review of lithium ion battery failure mechanisms and fire prevention strategies, Prog. Energy Combust. Sci. 73 (2019) 95–131, https://doi.org/10.1016/j.pecs.2019.03.002.

[5] J. Xu, Q. Duan, L. Zhang, Y. Liu, C. Zhao, Q. Wang, Experimental study of the cooling effect of water mist on 18650 lithium-ion battery at different initial temperatures, Process Saf. Environ. Prot. 157 (2022) 156–166, https://doi.org/10.1016/j.psep.2021.10.034.

[6] Z. Hu, B. Lei, Y. Li, Y. Shi, Q. Lei, Z. He, Comparative study on safety test and evaluation methods of lithium-ion batteries for energy storage, Energy Storage Sci. Technol. (2021), https://doi.org/10.19799/j.cnki.2095-4239.2021.0510.

[7] R. Zalosh, P. Gandhi, A. Barowy, Lithium-ion energy storage battery explosion incidents, J. Loss Prev. Process Ind. 72 (2021), 104560, https://doi.org/10.1016/j.jlp.2021.104560.

[8] D.P. Finegan, M. Scheel, J.B. Robinson, B. Tjaden, I. Hunt, T.J. Mason, et al., In-operando high-speed tomography of lithium-ion batteries during thermal runaway, Nat. Commun. 6 (2015) 6924, https://doi.org/10.1038/ncomms7924.

[9] X. Meng, S. Li, W. Fu, Y. Chen, Q. Duan, Q. Wang, Experimental study of intermittent spray cooling on suppression for lithium iron phosphate battery fires 11 (2022), 100142, https://doi.org/10.1016/j.etran.2021.100142.

[10] X. Lai, S. Wang, H. Wang, Y. Zheng, X. Feng, Investigation of thermal runaway propagation characteristics of lithium-ion battery modules under different trigger modes, Int. J. Heat Mass Transf. 171 (2021), 121080, https://doi.org/10.1016/j.ijheatmasstransfer.2021.121080.

[11] J. Bai, Z. Wang, T. Gao, W. Bai, J. Wang, Effect of mechanical extrusion force on thermal runaway of lithium-ion batteries caused by flat heating, J. Power Sources 507 (2021), 230305, https://doi.org/10.1016/j.jpowsour.2021.230305.

[12] Z. Huang, H. Li, W. Mei, C. Zhao, J. Sun, Q. Wang, Thermal runaway behavior of lithium iron phosphate battery during penetration, Fire. Technol 56 (6) (2020) 2405–2426, https://doi.org/10.1007/s10694-020-00967-1.

[13] Z. Huang, C. Zhao, H. Li, W. Peng, Z. Zhang, Q. Wang, Experimental study on thermal runaway and its propagation in the large format lithium ion battery module with two electrical connection modes, Energy 205 (2020), 117906, https://doi.org/10.1016/j.energy.2020.117906.

[14] H. Wang, W. Shi, F. Hu, Y. Wang, X. Hu, H. Li, Over-heating triggered thermal runaway behavior for lithium-ion battery with high nickel content in positive electrode, Energy 224 (2021), 120072, https://doi.org/10.1016/j.energy.2021.120072.

[15] Z. Huang, J. Liu, H. Zhai, Q. Wang, Experimental investigation on the characteristics of thermal runaway and its propagation of large-format lithium ion batteries under overcharging and overheating conditions, Energy 233 (2021), 121103, https://doi.org/10.1016/j.energy.2021.121103.

[16] C.J. Wang, Y.L. Zhu, F. Gao, C. Qi, P.L. Zhao, Q.F. Meng, et al., Thermal runaway behavior and features of LiFePO4 /graphite aged batteries under overcharge, Int. J. Energy Res. 44 (7) (2020) 5477–5487, https://doi.org/10.1002/er.5298.

[17] L. Sun, C. Wei, D. Guo, J. Liu, Z. Zhao, Z. Zheng, et al., Comparative study on thermal runaway characteristics of lithium iron phosphate battery modules under different overcharge conditions, Fire. Technol 56 (4) (2020) 1555–1574, https://doi.org/10.1007/s10694-019-00942-5.

[18] P. Liu, C. Liu, K. Yang, M. Zhang, F. Gao, B. Mao, et al., Thermal runaway and fire behaviors of lithium iron phosphate battery induced by over heating, J. Energy Storage 31 (2020), 101714, https://doi.org/10.1016/j.est.2020.101714.

[19] P.J. Bugryniec, J.N. Davidson, D.J. Cumming, S.F. Brown, Pursuing safer batteries: thermal abuse of LiFePO4 cells, J. Power Sources 414 (2019) 557–568, https://doi.org/10.1016/j.jpowsour.2019.01.013.

[20] D. Ren, X. Feng, L. Lu, X. He, M. Ouyang, Overcharge behaviors and failure mechanism of lithium-ion batteries under different test conditions, Appl. Energy 250 (2019) 323–332, https://doi.org/10.1016/j.apenergy.2019.05.015.

[21] Z. Huang, T. Shen, K. Jin, J. Sun, Q. Wang, Heating power effect on the thermal runaway characteristics of large-format lithium ion battery with Li(Ni1/3Co1/3Mn1/3)O2 as cathode, Energy 239 (2022), 121885, https://doi.org/10.1016/j.energy.2021.121885.

[22] P. Qin, J. Sun, Q. Wang, A new method to explore thermal and venting behavior of lithium-ion battery thermal runaway, J. Power Sources 486 (2021), 229357, https://doi.org/10.1016/j.jpowsour.2020.229357.

[23] T.-Y. Hsieh, Y.-S. Duh, C.-S. Kao, Evaluation of thermal hazard for commercial 14500 lithium-ion batteries, J. Therm. Anal. Calorim. 116 (3) (2014) 1491–1495, https://doi.org/10.1007/s10973-014-3755-x.

[24] Y.-S. Duh, J.-H. Theng, C.-C. Chen, C.-S. Kao, Comparative study on thermal runaway of commercial 14500, 18650 and 26650 LiFePO4 batteries used in electric vehicles, J. Energy Storage 31 (2020), 101580, https://doi.org/10.1016/j.est.2020.101580.

[25] A.W. Golubkov, D. Fuchs, J. Wagner, H. Wiltsche, C. Stangl, G. Fauler, et al., Thermal-runaway experiments on consumer li-ion batteries with metal-oxide and olivin-type cathodes, RSC Adv. 4 (7) (2014) 3633–3642, https://doi.org/10.1039/c3ra45748f.

[26] Z. Zhou, X. Zhou, D. Wang, M. Li, B. Wang, L. Yang, et al., Experimental analysis of lengthwise/transversal thermal characteristics and jet flow of large-format prismatic lithium-ion battery, Appl. Therm. Eng. 195 (2021), 117244, https://doi.org/10.1016/j.applthermaleng.2021.117244.

[27] B. Mao, C. Liu, K. Yang, S. Li, P. Liu, M. Zhang, et al., Thermal runaway and fire behaviors of a 300 ah lithium ion battery with LiFePO4 as cathode, Renew. Sust. Energ. Rev. 139 (2021), 110717, https://doi.org/10.1016/j.rser.2021.110717.

[28] Z. Wang, H. Yang, Y. Li, G. Wang, J. Wang, Thermal runaway and fire behaviors of large-scale lithium ion batteries with different heating methods, J. Hazard. Mater. 379 (2019), 120730, https://doi.org/10.1016/j.jhazmat.2019.06.007.

[29] L. Yuan, T. Dubaniewicz, I. Zlochower, R. Thomas, N. Rayyan, Experimental study on thermal runaway and vented gases of lithium-ion cells, Process Saf. Environ. Prot. 144 (2020) 186–192, https://doi.org/10.1016/j.psep.2020.07.028.

[30] Z. Jia, P. Qin, Z. Li, Z. Wei, K. Jin, L. Jiang, et al., Analysis of gas release during the process of thermal runaway of lithium-ion batteries with three different cathode materials, J. Energy Storage 50 (2022), 104302, https://doi.org/10.1016/j.est.2022.104302.

[31] Y.-B. He, G.-W. Ling, Z.-Y. Tang, Q.-S. Song, Q.-H. Yang, W. Chen, et al., Safety properties of liquid state soft pack high power batteries with carbon-coated LiFePO4/graphite electrodes, J. Solid State Electrochem. 14 (5) (2009) 751–756, https://doi.org/10.1007/s10008-009-0849-7.

[32] S.-i. Tobishim, J.-i. Yamaki, A consideration of lithium cell safety, J. Power Sources 81 (1999) 882–886, https://doi.org/10.1016/S0378-7753(98)00240-7.

[33] T. Shan, Z. Wang, X. Zhu, H. Wang, Y. Zhou, Y. Wang, et al., Explosion behavior investigation and safety assessment of large-format lithium-ion pouch cells, J. Energy Chem. 72 (2022) 241–257, https://doi.org/10.1016/j.jechem.2022.04.018.
[34] D. Belov, M.-H. Yang, Failure mechanism of li-ion battery at overcharge conditions, J. Solid State Electrochem. 12 (7–8) (2007) 885–894, https://doi.org/10.1007/s10008-007-0449-3.
[35] X. Zhu, Z. Wang, Y. Wang, H. Wang, C. Wang, L. Tong, et al., Overcharge investigation of large format lithium-ion pouch cells with Li(Ni0.6Co0.2Mn0.2)O2 cathode for electric vehicles: thermal runaway features and safety management method, Energy 169 (2019) 868–880, https://doi.org/10.1016/j.energy.2018.12.041.
[36] C. Uhlmann, J. Illig, M. Ender, R. Schuster, E. Ivers-Tiffée, In situ detection of lithium metal plating on graphite in experimental cells, J. Power Sources 279 (2015) 428–438, https://doi.org/10.1016/j.jpowsour.2015.01.046.
[37] Z. Wang, J. Yuan, X. Zhu, H. Wang, L. Huang, Y. Wang, et al., Overcharge-to-thermal-runaway behavior and safety assessment of commercial lithium-ion cells with different cathode materials: a comparison study, J. Energy Chem. 55 (2021) 484–498, https://doi.org/10.1016/j.jechem.2020.07.028.
[38] J. Ye, H. Chen, Q. Wang, P. Huang, J. Sun, S. Lo, Thermal behavior and failure mechanism of lithium ion cells during overcharge under adiabatic conditions, Appl. Energy 182 (2016) 464–474, https://doi.org/10.1016/j.apenergy.2016.08.124.
[39] C.J. Orendorff, The role of separators in lithium-ion cell safety, Electrochem. Soc. Interface 21 (2) (2012) 61–65, https://doi.org/10.1149/2.F07122if.
[40] E.P. Roth, D.H. Doughty, D.L. Pile, Effects of separator breakdown on abuse response of 18650 li-ion cells, J. Power Sources 174 (2) (2007) 579–583, https://doi.org/10.1016/j.jpowsour.2007.06.163.
[41] C. Qi, Y.-L. Zhu, F. Gao, K. Yang, Q.-J. Jiao, Morphology, structure and thermal stability analysis of cathode and anode material under overcharge, J. Electrochem. Soc. 165 (16) (2018) A3985–A3992, https://doi.org/10.1149/2.0911816jes.
[42] P. Liu, S. Li, K. Jin, W. Fu, C. Wang, Z. Jia, Thermal runaway and fire behaviors of large format Lithium Iron Phosphate battery induced by overheating and overcharging, Fire. Technol. 2 (2023) 1287, https://doi.org/10.1007/s10694-022-01287-2.
[43] Z. Huang, X. Li, Q. Wang, Q. Duan, Y. Li, L. Li, et al., Experimental investigation on thermal runaway propagation of large format lithium ion battery modules with two cathodes, Int. J. Heat Mass Transf. 172 (2021), 121077, https://doi.org/10.1016/j.ijheatmasstransfer.2021.121077.
[44] R. Spotnitz, J. Franklin, Abuse behavior of high-power, lithium-ion cells, J. Power Sources 113 (2003) 81–100, https://doi.org/10.1016/S0378-7753(02)00488-3.
[45] K. Zaghib, J. Dubé, A. Dallaire, K. Galoustov, A. Guerfi, M. Ramanathan, et al., Enhanced thermal safety and high power performance of carbon-coated LiFePO4 olivine cathode for li-ion batteries, J. Power Sources 219 (2012) 36–44, https://doi.org/10.1016/j.jpowsour.2012.05.018.
[46] Z. Liao, S. Zhang, Y. Zhao, Z. Qiu, K. Li, D. Han, et al., Experimental evaluation of thermolysis-driven gas emissions from LiPF6-carbonate electrolyte used in lithium-ion batteries, J. Energy Chem. 49 (2020) 124–135, https://doi.org/10.1016/j.jechem.2020.01.030.
[47] H. Yang, X.-D. Shen, Dynamic TGA–FTIR studies on the thermal stability of lithium/graphite with electrolyte in lithium-ion cell, J. Power Sources 167 (2) (2007) 515–519, https://doi.org/10.1016/j.jpowsour.2007.02.029.
[48] Gachot Gg, P.R. Re, D. Mathiron, S. Grugeon, M. Armand, J.-B. Leriche, Gas chromatography/mass spectrometry as a suitable tool for the Li-Ion battery electrolyte degradation mechanisms study, Anal. Chem. 83 (2011) 478–485, https://doi.org/10.1021/ac101948u.
[49] H. Yoshida, T. Fukunaga, T. Hazama, M. Terasaki, M. Mizutani, M. Yamachi, Degradation mechanism of alkyl carbonate solvents used in lithium-ion cells during initial charging, J. Power Sources 68 (1997) 311–315, https://doi.org/10.1016/S0378-7753(97)02635-9.
[50] A.D. Pasquier, F. Disma, T. Bowmer, A.S. Gozdz, G. Amatucci, J.-M. Tarascon, Differential scanning calorimetry study of the reactivity of carbon anodes in plastic li-ion batteries, J. Electrochem. Soc. 145 (1998) 472–477, https://doi.org/10.1149/1.1838287.
[51] D. Aurbach, A. Zaban, Y. Gofer, Y.E. Ely, I. Weissman, O. Chusid, et al., Recent studies of the lithium-liquid electrolyte interface electrochemical, morphological and spectral studies of a few important systems, J. Power Sources 54 (1995) 76–84, https://doi.org/10.1016/0378-7753(94)02044-4.
[52] C.-H.H. Jee-Sun Shin, Un-Ho Jung, Shung-Ik Lee, Hyeong-Jin Kim, Keon Kim, Effect of Li2CO3 additive on gas generation in lithium-ion batteries, J. Power Sources 109 (2002) 47–52, https://doi.org/10.1016/S0378-7753(02)00039-3.
[53] P. Ping, Q. Wang, P. Huang, K. Li, J. Sun, D. Kong, et al., Study of the fire behavior of high-energy lithium-ion batteries with full-scale burning test, J. Power Sources 285 (2015) 80–89, https://doi.org/10.1016/j.jpowsour.2015.03.035.
[54] H. Wang, A. Tang, K. Huang, Thermal behavior investigation of LiNi1/3Co1/3Mn1/3O2-based li-ion battery under overcharged test, Chin. J. Chem. 29 (2011) 27–32, https://doi.org/10.1002/cjoc.201190056.
[55] P. Qin, Z. Jia, J. Wu, K. Jin, Q. Duan, L. Jiang, et al., The thermal runaway analysis on LiFePO4 electrical energy storage packs with different venting areas and void volumes, Appl. Energy 313 (2022), 118767, https://doi.org/10.1016/j.apenergy.2022.118767.
[56] Y. Peng, L. Yang, X. Ju, B. Liao, K. Ye, L. Li, et al., A comprehensive investigation on the thermal and toxic hazards of large format lithium-ion batteries with LiFePO4 cathode, J. Hazard. Mater. 381 (2020), 120916, https://doi.org/10.1016/j.jhazmat.2019.120916.